Toxicology Letters 352 (2021) 54–60

Contents lists available at ScienceDirect

Toxicology Letters

journal homepage: www.elsevier.com/locate/toxlet

Whole brain *in vivo* neuropathology: Imaging site-specific changes in brain structure over time following trimethyltin exposure in rats

Praveen Kulkarni[a], Nicole Bens[a], Dhruv K. Karia[a], Craig F. Ferris[a,b,*]

[a] Center for Translational NeuroImaging, Northeastern University, Boston, MA, United States
[b] Psychology and Pharmaceutical Sciences, Northeastern University, Boston, MA, United States

HIGHLIGHTS

- "In vivo neuropathology" is an imaging protocol that can identify sites of neuroinflammation across the entire brain.
- This non-invasive imaging protocol allows studies on time-dependent neuropathology.
- The global maps of neurotoxic injury can be used to guide the histopathology during preclinical drug development.
- Analysis is achieved with a minimum number of rats in compliance with the humane care and use of laboratory animals.
- "In vivo neuropathology" provides an alternative to the traditional tests for assessing drug neurotoxicity.
- "In vivo neuropathology" can minimize the cost of preclinical CNS toxicology.

ARTICLE INFO

Article history:
Received 22 April 2021
Received in revised form 9 September 2021
Accepted 27 September 2021
Editor: Dr. Angela Mally
Available online 29 September 2021

Keywords:
Diffusion weighted imaging
Apparent diffusion coefficient
Indices of anisotropy
Cerebellum
Hippocampus
Cerebral cortex

ABSTRACT

Presented is a diffusion weighted imaging protocol with measures of apparent diffusion coefficient which when registered to a 3D MRI rat brain atlas provides site-specific information on 173 different brain areas. This protocol coined "in vivo neuropathology" was used to follow the progressive neurotoxic effects of trimethyltin on global gray matter microarchitecture. Four rats were given an IP injection of 7 mg/kg of the neurotoxin trimethyltin and imaged for changes in water diffusivity at 3- and 7-days post injections. At 3 days, there was a significant decrease in apparent diffusion coefficient, a proxy for cytotoxic edema, in several cortical areas and cerebellum. At 7 days the level of injury expanded to include most of the cerebral cortex, hippocampus, olfactory system, and cerebellum/brainstem corroborating much of the work done with traditional histopathology. Analysis is achieved with a minimum number of rats adhering to the laws and regulations around the humane care and use of laboratory animals, providing an alternative to the traditional tests for assessing drug neurotoxicity. "In vivo neuropathology" can minimize the cost, expedite the process, and identify subtle changes in site-specific brain micro-architecture across the entire brain.

1. Introduction

In a study on traumatic brain injury we developed a imaging protocol called "In Vivo Neuropathology" to identify common sites of brain neuroinflammation following unilateral injury to the front or back of the brain (Kulkarni et al., 2015). Using voxel-based diffusion weighted imaging (DWI) with different measures of anisotropy mapped to a 3D rat brain atlas we were able to identify subtle changes in neuroinflammation at common unilateral sites in the hippocampus, thalamus, and central amygdala regardless of where the brain was injured. In a more recent study, we used the same imaging protocol but focused on only one measure of DWI, the apparent diffusion coefficient (ADC) to following changes in cerebral edema following a single mild head impact (Kulkarni et al., 2020). ADC is quantitative measure of water mobility commonly used in neuroradiology to assess cytotoxic edema (Toth, 2015). Cytotoxic edema is characterized by cellular swelling at the site of injury resulting in a reduced measure of ADC (Hudak et al., 2014).

* Corresponding author at: Department of Psychology, Northeastern University, 125 NI Hall, 360 Huntington Ave, Boston, MA, 02115-5000, United States.
E-mail address: c.ferris@northeastern.edu (C.F. Ferris).

http://dx.doi.org/10.1016/j.toxlet.2021.09.009

This was an exploratory study using DWI and ADC to map the progression of injury to the whole brain following treatment with trimethyltin (TMT), a well characterized rat model used in preclinical studies to follow lesions in the cortex and hippocampus (Roberts et al., 2015). Safety pharmacology particularly in area neurotoxicology is critical in any early drug discovery program. Indeed many candidate molecules fail in preclinical studies and early clinical trials because of issues of structural and functional neurotoxicity (Walker et al., 2018). Evidence of structural damage is traditionally assessed on postmortem tissue by time consuming histopathology (Rao et al., 2011, 2014). The injury to the brain is sampled at a single time point in disease progression and evaluated in predetermined brain areas that represent only a fraction of the CNS. Reported here is a method for imaging structural changes reflecting neuroinflammation and cytotoxic edema across 173 different brain areas in the same animals 3 and 7 days after TMT treatment. This global perspective tracking time-dependent neuropathology can be achieved with a minimum of rats adhering to the laws and regulations around the humane care and use of laboratory animals, providing an alternative to the traditional tests for assessing drug neurotoxicity.

2. Materials and methods

Four male Sprague Dawley rats (ca 350 gm) were obtained from Charles River Laboratories (Wilmington, Massachusetts, USA). Rats were housed two per cage, maintained on a 12:12 h light-dark cycle with lights on at 07:00 h and allowed access to food and water ad libitum. All rats were acquired and cared for in accordance with the guidelines published in the Guide for the Care and Use of Laboratory Animals (National Institutes of Health Publications No. 85–23, Revised 1985) and adhered to the National Institutes of Health and the American Association for Laboratory Animal Science guidelines. The protocols used in this study complied with the regulations of the Institutional Animal Care and Use Committee at the Northeastern University and adhere to the ARRIVE guidelines for reporting in vivo experiments in animal research (Kilkenny et al., 2010). Following pre-scan, rats were treated with a single IP injection of 7 mg/kg dose volume (ca 0.3 mL) of trimethyltin chloride (Sigma-Aldrich Inc, St Louis MO) and returned to their home cage to be left undisturbed until imaged on days 3 and 7 post injection.

2.1. Neuroimaging

Imaging sessions were conducted using a Bruker Biospec 7.0 T/20-cm USR horizontal magnet (Bruker, Billerica, MA, USA) and a 20-G/cm magnetic field gradient insert (ID = 12 cm) capable of a 120-μs rise time. Radio frequency signals were sent and received with a quadrature volume coil built into the animal restrainer (Ekam Imaging Inc, Boston, MA, USA). The design of the restraining system included a padded head support obviating the need for ear bars helping to reduce animal discomfort while minimizing motion artifact. All rats were imaged under 1%(± 0.5) isoflurane while keeping a respiratory rate of 50–60 breaths/min.

Diffusion Weighted Imaging – Quantitative Anisotropy

DWI was acquired with a 3D spin-echo echo-planar-imaging (3D-EPI) pulse sequence having the following parameters: TR/TE = 500/20 msec, eight EPI segments, and 10 non-collinear gradient directions with a single b-value shell at 1000s/mm^2 and one image with a B-value of 0 s/mm^2 (referred to as B0) as previously described (Cai et al., 2019; Ferris et al., 2019; Kulkarni et al., 2019). Geometrical parameters were: 48 coronal slices, each 0.313 mm thick (brain volume) and with in-plane resolution of 0.313 × 0.313 mm^2 (matrix size 96 × 96; FOV 30 mm^3). The imaging protocol was repeated two times for signal averaging. Each DWI acquisition took 45 min and the entire MRI protocol including the anatomy lasted about 90 min. There are numerous studies detailing the benefits of multi-shot EPI in BOLD imaging (Hoogenraad et al., 2000; Kang et al., 2015; Menon et al., 1997; Poser and Norris, 2009; Swisher et al., 2012). We avoided using single shot EPI because of its sever geometrical distortion at high field strengths (≥7 T) and loss of effective spatial resolution as the readout period increases (Farzaneh et al., 1990; Hoogenraad et al., 2000; Jesmanowicz et al., 1998). There is also the possibility of signal loss in single shot EPI due to accumulated magnetic susceptibility or field inhomogeneity (Kang et al., 2015).

DWI analysis was completed with MATLAB and MedINRIA (1.9.0; http://www-sop.inria.fr/asclepios/software/MedINRIA/index.php) software. Because sporadic excessive breathing during DWI acquisition can lead to significant image motion artifacts that are apparent only in the slices sampled when motion occurred, each image (for each slice and each gradient direction) was screened prior to DWI analysis. If we found motion in more than one pixel length (ca 300 μm) in any direction that subject was eliminated from the analyses. No subjects were eliminated in this study. For statistical comparisons among rats, each brain volume was registered to the 3D MRI rat brain atlas allowing voxel- and region-based statistics. All image transformations and statistical analyses were carried out using the in-house EVA software (Ekam Solutions LLC, Boston MA). For each rat, the B0 image was co-registered with the MRI atlas using a 9-parameter affine transformation. Insight tool kit (https://itk.org/) registration framework was used with Affine transformation, mutual information similarity matrix and gradient descent optimizer with following parameters: Max step length 0.3 mm, Min step length 0.0001 mm, Number of iterations 100, Scan threshold 20 %. Finally, before segmentation registration was closely inspected for quality and manually corrected if necessary. The average value for each ROI was computed using map files for indices of apparent diffusion coefficient (ADC) and fractional anisotropy (FA).

Statistical differences in measures of DWI between experimental groups were determined using a nonparametric Kruskal Wallis multiple comparisons test (critical value set at <0.05) followed by post hoc analyses using a Wilcoxon rank-sum test for individual differences. The formula below was used to account for false discovery from multiple comparisons.

$$P_{(i)} \leq \frac{i \quad q}{\nu c(V)}$$

P(i) is the *p* value based on the *t* test analysis. The false-positive filter value *q* was set to 0.2 and the predetermined *c(V)* was set to unity (Benjamini and Hochberg, 1995). The corrected probability is noted on each table.

2.2. Histology

Three male rats were treated with TMT and one week later transcardially perfused with 4% paraformaldehyde. The brains were removed and processed for cryo-embedding. Coronal brain sections 40 u M thick were generated using a Leica CM1520 cryostat and collected on Colorfrost slides, air dried and stored at −80*C. Brain sections are washed in PBS twice and incubated in a blocking buffer (PBS pH 7.4, 5 % NGS, 0.3 % Triton X-100) for 1 h. The primary antibody rabbit anti-glial fibrillary acidic protein (1:1000, DAKO) was applied for 1 h at 4*C in incubation solution (PBS pH 7.4, 1 % BSA, 1 % NGS, 0.1 % Triton X-100). Following the

Table 1
Apparent Diffusion Coefficient Day Three Post TMT Treatment.

	Pre TMT			3 Day Post TMT			
Brain Area	Ave	SD		Ave	SD	P-val	ω Sq
superior colliculus	2.63	0.16	>	2.04	0.33	0.020	0.706
6th cerebellar lobule	2.44	0.24	>	1.91	0.15	0.021	0.695
lateral posterior thalamus	2.51	0.10	>	1.89	0.32	0.021	0.695
primary motor ctx	2.37	0.19	>	1.98	0.22	0.021	0.695
secondary motor ctx	2.60	0.24	>	2.11	0.18	0.021	0.695
simple lobule cerebellum	2.47	0.28	>	1.99	0.28	0.021	0.695
crus 1 of ansiform lobule	2.16	0.39	>	1.70	0.23	0.042	0.489
anterior thalamus	2.15	0.13	>	1.80	0.22	0.043	0.481
anterior cingulate ctx	2.41	0.25	>	2.01	0.22	0.043	0.481
dorsal medial striatum	2.07	0.12	>	1.80	0.16	0.043	0.481
frontal association ctx	2.57	0.20	>	2.15	0.31	0.043	0.481
medial dorsal thalamus	2.14	0.13	>	1.82	0.27	0.043	0.481
periaqueductal gray	2.56	0.27	>	2.12	0.34	0.043	0.481
parietal ctx	2.43	0.08	>	2.06	0.26	0.043	0.481
primary ss ctx forelimb	2.24	0.15	>	1.93	0.26	0.043	0.481
primary ss ctx trunk	2.45	0.13	>	2.10	0.26	0.043	0.481
visual 1 ctx	2.33	0.23	>	1.94	0.28	0.043	0.481

brains are washed, then the secondary antibody goat anti-rabbit conjugated with AF-488 (Invitrogen) is applied for 1 h. The slides are mounted using Vectashield infused with DAPI (Vector Lab, Burlingame) for nuclei visualization. Brain sections were observed using the Zeiss LSM 800 microscope. All following measurements on images were conducted using ImageJ.

3. Results

Show in Table 1 are 18 out of173 brain areas with significantly reduced measures of ADC 3 days following TMT exposure. The brain areas are ranked in order of their significance (P-val) and effect size (omega square; ω Sq). Shown are the average (Ave, gray columns) and standard deviation (SD) for the four rats. Note that all brain areas following TMT have ADC values lower than normal a possible sign of cytotoxic edema. In many cases the SD is less than 5% of the sample average demonstrating that a small sample size is adequate and sufficient to show site-specific neuropathology using DWI and ADC/RD values as a proxy for cytogenic edema. The areas primarily affected are localized to the cerebral cortex (ctx) (e.g. motor, somatosensory (ss), anterior cingulate, parietal, and visual cortices) cerebellum, (e.g. 6th cerebellar lobule, simple lobule, and crus 1 lobule and thalamus (e.g. dorsal medial, lateral posterior and anterior) as depicted in Fig. 1. With time the neuropathology expands across more of the brain as reported in Table 2 and shown in Fig. 1.

Shown in Table 2 are 45/173 brain areas with significantly reduced measures of ADC on day 7 following TMT exposure. Again, all ADC values are lower than baseline. The hippocampus, e.g. CA3, CA1, CA2 and dentate gyrus is significantly affected with high effect sizes. The olfactory bulb comprised of the external plexiform layer and granular layer is also highly affected. There were few significant changes in brain microarchitecture as measured by FA for either 3-days (4/173 brain areas) and 7-days (2/173) post

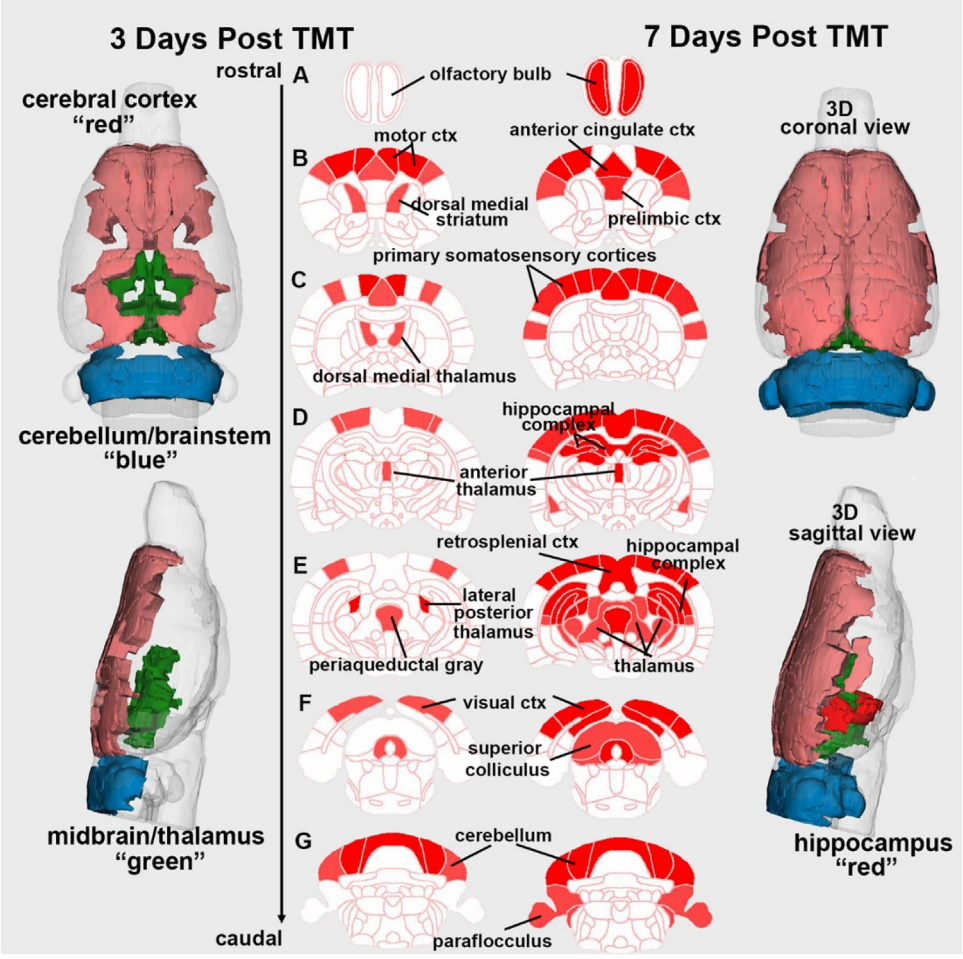

Fig. 1. Anatomical localizations of neurotoxic injury.
2D maps show the sites of neurotoxic injury at 3-days (left) and 7-days (right) following TMT treatment. The 3D images are a summary of these brain areas.

Table 2
Apparent Diffusion Coefficient Seven Days Post TMT Treatment.

	Pre TMT			7 Day Post TMT			
Brain Area	Ave	SD		Ave	SD	P-val	ω Sq
crus 1 of ansiform lobule	2.16	0.39	>	1.62	0.10	0.020	0.706
lateral dorsal thalamus	2.24	0.26	>	1.80	0.13	0.020	0.706
medial septum	2.17	0.17	>	1.83	0.10	0.020	0.706
superior colliculus	2.63	0.16	>	2.03	0.19	0.020	0.706
visual 1 ctx	2.33	0.23	>	1.97	0.12	0.020	0.706
6th cerebellar lobule	2.44	0.24	>	1.90	0.19	0.021	0.695
CA1 dorsal	2.31	0.16	>	1.88	0.17	0.021	0.695
CA3 dorsal	2.32	0.23	>	1.87	0.13	0.021	0.695
anterior cingulate ctx	2.41	0.25	>	1.94	0.11	0.021	0.695
crus 2 of ansiform lobule	2.08	0.31	>	1.52	0.21	0.021	0.695
dentate gyrus dorsal	2.40	0.20	>	1.94	0.10	0.021	0.695
external plexiform layer	2.26	0.11	>	2.04	0.06	0.021	0.695
granular cell layer	2.19	0.11	>	1.91	0.04	0.021	0.695
lateral geniculate	2.22	0.23	>	1.81	0.10	0.021	0.695
lateral posterior thalamus	2.51	0.10	>	1.97	0.08	0.021	0.695
primary motor ctx	2.37	0.19	>	1.90	0.03	0.021	0.695
periaqueductal gray	2.56	0.27	>	2.06	0.12	0.021	0.695
parabrachial nucleus	2.45	0.38	>	1.90	0.16	0.021	0.695
parietal ctx	2.43	0.08	>	1.99	0.20	0.021	0.695
raphe obscurus nucleus	2.66	0.27	>	2.19	0.18	0.021	0.695
retrosplenial caudal ctx	2.54	0.16	>	2.27	0.04	0.021	0.695
retrosplenial rostral ctx	2.62	0.31	>	2.14	0.16	0.021	0.695
primary ss ctx forelimb	2.24	0.15	>	1.84	0.09	0.021	0.695
primary ss ctx hindlimb	2.49	0.30	>	1.91	0.14	0.021	0.695
primary ss ctx trunk	2.45	0.13	>	1.97	0.19	0.021	0.695
simple lobule cerebellum	2.47	0.28	>	1.84	0.19	0.021	0.695
visual 2 ctx	2.25	0.18	>	1.93	0.21	0.021	0.695
prelimbic ctx	2.02	0.14	>	1.77	0.09	0.029	0.592
primary ss ctx barrel field	2.20	0.12	>	1.86	0.13	0.029	0.592
central gray	2.70	0.34	>	2.13	0.16	0.042	0.489
7th cerebellar lobule	2.26	0.38	>	1.65	0.37	0.043	0.481
anterior pretectal nucleus	2.23	0.23	>	1.84	0.27	0.043	0.481
CA2	2.20	0.20	>	1.88	0.20	0.043	0.481
CA3 hippocampus ventral	2.29	0.21	>	2.02	0.14	0.043	0.481
dorsomedial tegmentum	2.32	0.33	>	1.88	0.19	0.043	0.481
flocculus cerebellum	2.49	0.37	>	2.00	0.19	0.043	0.481
inferior colliculus	2.73	0.26	>	2.21	0.28	0.043	0.481
lateral amygdaloid nucleus	2.35	0.21	>	1.99	0.21	0.043	0.481
locus coeruleus	2.86	0.46	>	2.06	0.18	0.043	0.481
medial geniculate	2.25	0.37	>	1.82	0.15	0.043	0.481
paraflocculus cerebellum	2.32	0.27	>	1.92	0.13	0.043	0.481
reticular nucleus midbrain	2.36	0.32	>	1.88	0.16	0.043	0.481
primary ss ctx jaw	1.98	0.08	>	1.77	0.14	0.043	0.481
primary ss ctx shoulder	2.36	0.25	>	1.93	0.16	0.043	0.481
secondary ss ctx	2.00	0.19	>	1.69	0.14	0.043	0.481

TMT (see Supplementary Data Tables S2). Fig. 2 depicts bar graphs showing the mean and the range of the 173 brain areas for each time point for measures of ADC and FA.

Fig. 1 shows the locations of all brain areas mapped to the rat atlas that were significantly affected by TMT at 3- and 7-days post drug. The rows of 2D axial sections labeled A–E extend rostral to caudal, from olfactory bulbs to cerebellum, respectively. Of note are the 2nd motor ctx (B), dorsal medial striatum (B) and dorsal medial thalamus (C) that are affected at day 3 but not by day 7. The ADC values for each time point for each brain area were 2.60/2.11/2.15, 2.07/1.80/1.83, and 2.14/1.82/1.89, respectively. In all other brain areas the injury persists and exacerbates over time. The 3D color-coded images to the sides of each row are a summary of the brain areas affected by TMT at each time point.

Fig. 3 shows examples of elevated levels of glial fibrillary acidic protein (GFAP), a marker of astrocytic activation in the somatosensory cortex (panel a), cerebellum (b), and hippocampus (d) 7 days post TMT treatment. As a control, the caudate/putamen (c) was analyzed for GFAP staining as it was not identified as having any significant change in ADC values at this time point (see Table 2). The amygdala also showed no evidence of neuroinflammation (panel e). The brain illustration in each figure shows the approximate location (box) used for analysis. The analysis collected from multiple samples from these locations across contiguous brain sections are shown in the bar graphs. Both the cortex (somatosensory cortex), cerebellum (vermis, lobules 6 and 7) and hippocampus (CA3) show significantly greater GFAP signal contrast as compared to the caudate/putamen.

4. Discussion

Rats exposed to TMT is considered an ideal model for assessing neurotoxicity, causing a diffuse and widespread injury that has been well characterized, particularly with respect to its toxic effect on hippocampus and cortex (Balaban et al., 1988; Brown et al., 1979). This simple study on four rats using ADC values to assess CNS injury to TMT corroborated the data from several studies identifying the hippocampus and cortex as two of the most sensitive regions of the brain to TMT toxicity. The TMT-induced inflammation was confirmed by GFAP staining in these regions.

The neurons in the hippocampus, cortex and many of the other areas listed in Table 2 are known to be sensitive to the toxic effects

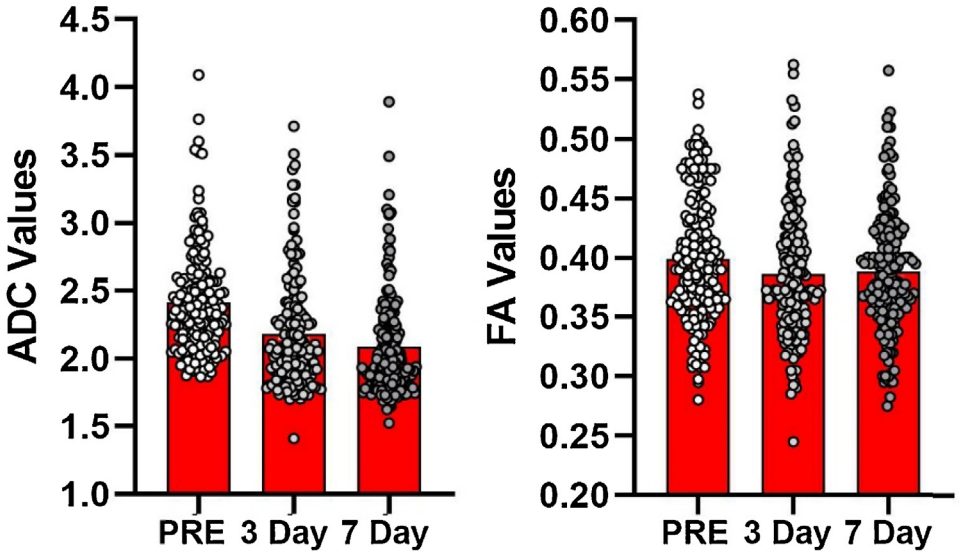

Fig. 2. Summary of whole brain ADC and FA values for each experimental time point.
Shown are bar graphs of the mean together with the range for each DWI measure for 173 brain areas for each time point. For apparent diffusion coefficient (ADC) mean and SD: Pre (2.41 ± 0.46); 3-Day (2.18 ± 0.57); 7-Day (2.08 ± 0.49). For fractional anisotropy (FA) mean and SD: Pre (0.39 ± 0.10); 3-Day (0.38 ± 0.07) 7-Day (0.38 ± 0.08)

of TMT; however, the cerebellum is not usually associated with TMT toxicity. Krady et al., using cDNA subtraction hybridization to characterize mRNA common to TMT sensitive neurons and reported intense hybridization signal in the granule layer of the cerebellum suggesting sensitivity to TMT that may not result in neuronal death (Krady et al., 1990). Interestingly, we confirmed the increased ADC values in the cerebellum 7 days post TMT were associated with an increase in GFAP staining in the 6/7 cerebellar lobules.

To the best of our knowledge there have only been two other studies using MRI to evaluate the neuropathology of TMT. Andjus and coworkers using a T2 weighted MRI protocol could only show a dilation of the lateral ventricle following TMT treatment in rats (Andjus et al., 2009). Johnson et.al., using a protocol called magnetic resonance histology, ex-vivo imaging of fixed brains, was only able to identify a few areas of TMT injury with DWI using a similar dose (7 mg/kg) and time course (3 days) used in this study (Johnson et al., 2014). These studies using MRI were unable to provide the sensitivity or sites specificity demonstrated here.

Interestingly, three brain areas were significantly different at 3 days but not 7 which may reflect a trend toward recovery or simply a casualty of statistics and Type 2 error because of the small sample size. Indeed, the small sample size of four rats would suggest just such an error. However, one of the major advantages to animal imaging is the homogeneity of the subject pool. Commercially breed strains of rats are essentially genetically identical. Using male rats of the same weight and age, as in this study, assures that the size and shape of the brains are indistinguishable. When registered into a 3D segmented, annotated rat atlas, the anatomical fidelity across subjects is highly conserved. In this study ca 20,000 isotropic voxels with different DWI measures were localized to one of 173 discrete 3D brain volumes. The variation between voxel numbers for brain area between subjects is usually less than 2 %. In this study the variance in the mean DWI values was extremely small where the SD was less than 10 % in a group of only four animals.

To test the likelihood of risk for Type 2 error we ran several brain areas with G*Power software that provides a power analysis based on known means and standard SDs. Using the means and SDs provided in Table 2 for Pre and 7-Day we calculated a sample size using a two-tailed test, with an alpha of 0.05, beta of 0.10, power of 0.90, and found that the dentate had an effect size (dz) of 2.65, with a recommended sample size of **4**. The same was true for the 6th cerebellar lobules (effect size 2.466, recommendation **4**). The primary somatosensory ctx hindlimb (effect size 3.05) had a recommendation of **3** for a sample size. In these cases the likelihood of making a Type II error is between 2–7 % with samples sizes of 3–4. However, it should be considered that TMT is a very toxic drug with a long history of pathohistological characterization within days of treatment. Any candidate in an early drug discovery program is unlikely to have such toxic side effects. "*In vivo* neuropathology" can minimize the cost, expedite the process, and identify subtle changes in site-specific brain microarchitecture across the entire brain. Since "*in vivo* neuropathology" is noninvasive and can be used to study disease progression, these studies on TMT could have extended over several more days or weeks providing much needed information on acute injury and recovery. Indeed, rats given a single 8 mg/kg dose of TMT can survive up to 180 days (Koczyk and Oderfeld-Nowak, 2000). This is a dilemma faced in any neurotoxicity study using traditional methods - when to look and where.

Using ADC as a surrogate marker of brain injury associated with edema is a point in case. The immediate exposure to TMT and onset of neuroinflammation could disrupt the blood brain barrier causing an initial phase of vasogenic edema and expansion of the extracellular fluid volume. This would result in an increase in ADC followed by cytogenic edema, cellular swelling due to loss of homeostatic regulation of osmolarity across the plasma membrane that results in lower ADC values as noted in this study. The timing and severity of this transition is dependent upon the level of brain injury.

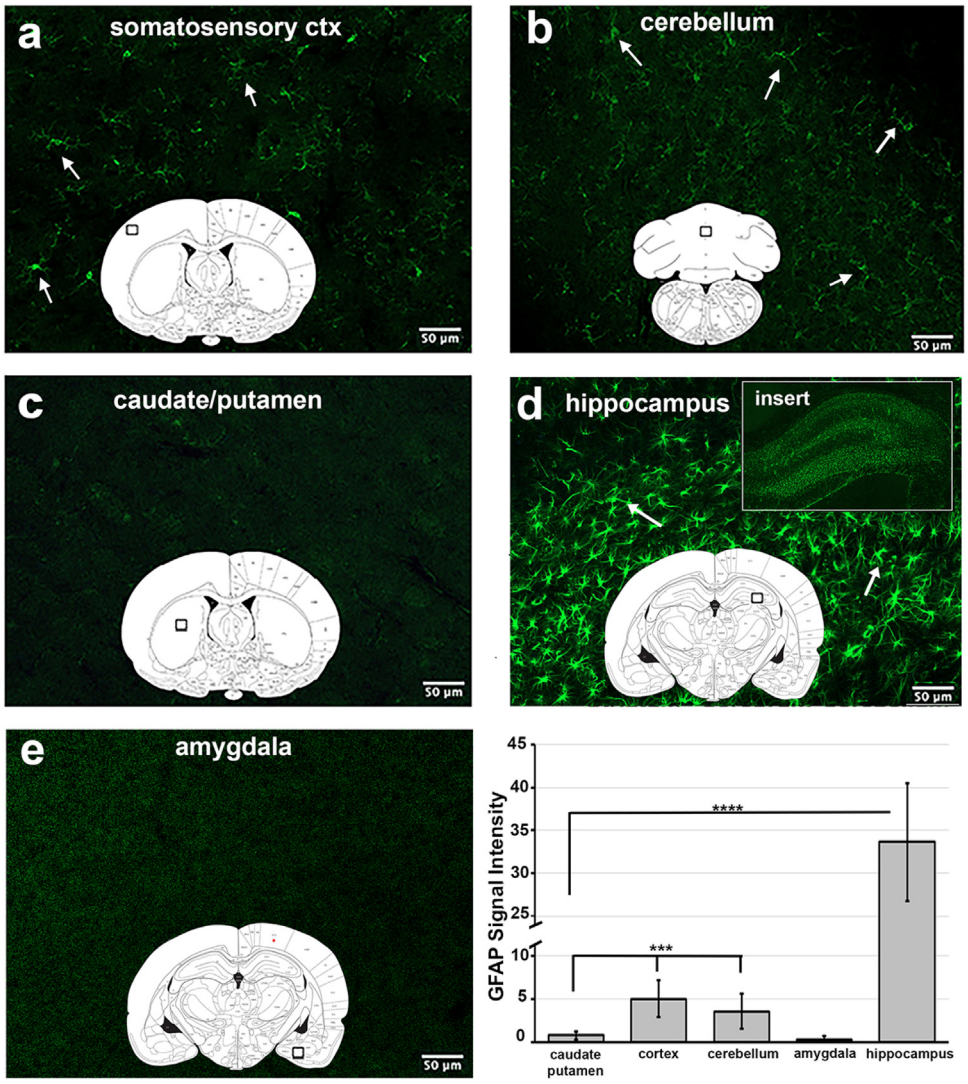

Fig. 3. GFAP staining in brain areas sensitive to TMT.
Shown are the activated astrocytes (arrows) in somatosensory cortex (a), cerebellum (b), hippocampus (d). The bar graphs show mean and SD of GFAP signal intensity for each brain regions sampled at the approximate site of the box in each frontal brain illustration. The insert in panel d shows the density of GFAP staining in astrocytes throughout the hippocampus Scale bar = 50 um, *** $p < 0.001$, **** $p < 0.0001$.

5. Conclusion

"In vivo neuropathology" is an imaging protocol using DWI and measures of ADC combined with computational analysis using a 3D MRI rat atlas with 173 brain areas to identify putative sites of neuroinflammation and edema following exposure to the neurotoxin TMT. This non-invasive imaging protocol allows studies on time-dependent neuropathology allowing researchers to know where and when to look for neurotoxic risk in early drug discovery programs. This readout can be achieved with a minimum of rats adhering to the laws and regulations around the humane care and use of laboratory animals, providing an alternative to the traditional tests for assessing drug neurotoxicity.

Ethics approval and consent to participate

Not applicable.

Consent for publication

Yes.

Availability of data and material

All data can be accessed through a link to Mendeley. DOI to follow.

Funding

None.

Authors' contributions

All of the authors have contributed substantially to the manuscript. All authors have read and agreed to the published version of the manuscript.

Concept, drafting and interpretation – Ferris and Kulkarni.

Execution and analysis – Kulkarni, Karia, Bens.

Declaration of Competing Interest

The authors declare the following financial interests/personal relationships which may be considered as potential competing

interests: Ferris has a financial interest in Ekam Imaging/Animal Imaging Research the company that manufactures the technology for imaging animals.

Acknowledgements

None.

Appendix A. Supplementary data

Supplementary material related to this article can be found, in the online version, at doi:https://doi.org/10.1016/j.toxlet.2021.09.009.

References

Andjus, P.R., Bataveljic, D., Vanhoutte, G., Mitrecic, D., Pizzolante, F., Djogo, N., Nicaise, C., Gankam Kengne, F., Gangitano, C., Michetti, F., van der Linden, A., Pochet, R., Bacic, G., 2009. In vivo morphological changes in animal models of amyotrophic lateral sclerosis and Alzheimer's-like disease: MRI approach. Anat. Rec. 292, 1882–1892.

Balaban, C.D., O'Callaghan, J.P., Billingsley, M.L., 1988. Trimethyltin-induced neuronal damage in the rat brain: comparative studies using silver degeneration stains, immunocytochemistry and immunoassay for neuronotypic and gliotypic proteins. Neuroscience 26, 337–361.

Benjamini, Y., Hochberg, Y., 1995. Controlling the false discovery rate: a practical and powerful approach to multiple testing. J. R. Stat. Soc. Ser. B (Methodological) 57, 289–300.

Brown, A.W., Aldridge, W.N., Street, B.W., Verschoyle, R.D., 1979. The behavioral and neuropathologic sequelae of intoxication by trimethyltin compounds in the rat. Am. J. Pathol. 97, 59–82.

Cai, X., Qiao, J., Knox, T., Iriah, S., Kulkarni, P., Madularu, D., Morrison, T., Waszczak, B., Hartner, J.C., Ferris, C.F., 2019. In search of early neuroradiological biomarkers for Parkinson's Disease: Alterations in resting state functional connectivity and gray matter microarchitecture in PINK1 -/- rats. Brain Res. 1706, 58–67.

Farzaneh, F., Riederer, S.J., Pelc, N.J., 1990. Analysis of T2 limitations and off-resonance effects on spatial resolution and artifacts in echo-planar imaging. Magn. Reson. Med. 14, 123–139.

Ferris, C.F., Nodine, S., Pottala, T., Cai, X., Knox, T.M., Fofana, F.H., Kim, S., Kulkarni, P., Crystal, J.D., Hohmann, A.G., 2019. Alterations in brain neurocircuitry following treatment with the chemotherapeutic agent paclitaxel in rats. Neurobiol. Pain 6, 100034.

Hoogenraad, F.G., Pouwels, P.J., Hofman, M.B., Rombouts, S.A., Lavini, C., Leach, M.O., Haacke, E.M., 2000. High-resolution segmented EPI in a motor task fMRI study. Magn. Reson. Imaging 18, 405–409.

Hudak, A.M., Peng, L., Marquez de la Plata, C., Thottakara, J., Moore, C., Harper, C., McColl, R., Babcock, E., Diaz-Arrastia, R., 2014. Cytotoxic and vasogenic cerebral oedema in traumatic brain injury: assessment with FLAIR and DWI imaging. Brain Injury: [BI] 28, 1602–1609.

Jesmanowicz, A., Bandettini, P.A., Hyde, J.S., 1998. Single-shot half k-space high-resolution gradient-recalled EPI for fMRI at 3 Tesla. Magn. Reson. Med. 40, 754–762.

Johnson, G.A., Calabrese, E., Little, P.B., Hedlund, L., Qi, Y., Badea, A., 2014. Quantitative mapping of trimethyltin injury in the rat brain using magnetic resonance histology. Neurotoxicology 42, 12–23.

Kang, D., Sung, Y.W., Kang, C.K., 2015. Fast imaging technique for fMRI: consecutive multishot echo planar imaging accelerated with GRAPPA technique. Biomed Res. Int. 2015, 394213.

Kilkenny, C., Browne, W.J., Cuthill, I.C., Emerson, M., Altman, D.G., 2010. Improving bioscience research reporting: the ARRIVE guidelines for reporting animal research. PLoS Biol. 8, e1000412.

Koczyk, D., Oderfeld-Nowak, B., 2000. Long-term microglial and astroglial activation in the hippocampus of trimethyltin-intoxicated rat: stimulation of NGF and TrkA immunoreactivities in astroglia but not in microglia. Int. J. Dev. Neurosci. 18, 591–606.

Krady, J.K., Oyler, G.A., Balaban, C.D., Billingsley, M.L., 1990. Use of avidin-biotin subtractive hybridization to characterize mRNA common to neurons destroyed by the selective neurotoxicant trimethyltin. Brain Res. Mol. Brain Res. 7, 287–297.

Kulkarni, P., Kenkel, W., Finklestein, S.P., Barchet, T.M., Ren, J., Davenport, M., Shenton, M.E., Kikinis, Z., Nedelman, M., Ferris, C.F., 2015. Use of anisotropy, 3D segmented atlas, and computational analysis to identify gray matter subcortical lesions common to concussive injury from different sites on the cortex. PLoS One 10, e0125748.

Kulkarni, P., Morrison, T.R., Cai, X., Iriah, S., Simon, N., Sabrick, J., Neuroth, L., Ferris, C. F., 2019. Neuroradiological changes following single or repetitive mild TBI. Front. Syst. Neurosci. 13, 34.

Kulkarni, P., Bhosle, M.R., Lu, S.F., Simon, N.S., Iriah, S., Brownstein, M.J., Ferris, C.F., 2020. Evidence of early vasogenic edema following minor head impact that can be reduced with a vasopressin V1a receptor antagonist. Brain Res. Bull. 165, 218–227.

Menon, R.S., Thomas, C.G., Gati, J.S., 1997. Investigation of BOLD contrast in fMRI using multi-shot EPI. NMR Biomed. 10, 179–182.

Poser, B.A., Norris, D.G., 2009. Investigating the benefits of multi-echo EPI for fMRI at 7 T. NeuroImage 45, 1162–1172.

Rao, D.B., Little, P.B., Malarkey, D.E., Herbert, R.A., Sills, R.C., 2011. Histopathological evaluation of the nervous system in National Toxicology Program rodent studies: a modified approach. Toxicol. Pathol. 39, 463–470.

Rao, D.B., Little, P.B., Sills, R.C., 2014. Subsite awareness in neuropathology evaluation of National Toxicology Program (NTP) studies: a review of select neuroanatomical structures with their functional significance in rodents. Toxicol. Pathol. 42, 487–509.

Roberts, R.A., Aschner, M., Calligaro, D., Guilarte, T.R., Hanig, J.P., Herr, D.W., Hudzik, T.J., Jeromin, A., Kallman, M.J., Liachenko, S., Lynch 3rd, J.J., Miller, D.B., Moser, V. C., O'Callaghan, J.P., Slikker Jr., W., Paule, M.G., 2015. Translational biomarkers of neurotoxicity: a health and environmental sciences institute perspective on the way forward. Toxicol. Sci. 148, 332–340.

Swisher, J.D., Sexton, J.A., Gatenby, J.C., Gore, J.C., Tong, F., 2012. Multishot versus single-shot pulse sequences in very high field fMRI: a comparison using retinotopic mapping. PLoS One 7, e34626.

Toth, A., 2015. Magnetic resonance imaging application in the Area of mild and acute traumatic brain injury: implications for diagnostic markers? In: Kobeissy, F.H. (Ed.), Brain Neurotrauma: Molecular, Neuropsychological, and Rehabilitation Aspects, Boca Raton (FL), .

Walker, A.L., Imam, S.Z., Roberts, R.A., 2018. Drug discovery and development: biomarkers of neurotoxicity and neurodegeneration. Exp. Biol. Med. (Maywood) 243, 1037–1045.